DNS simulation and analysis of periodic planar liquid sheet assisted atomization

Matthias Averseng, Davide Zuzio, Athanasios Boutsikakis, Jean-Luc Estivalèzes

DNS simulation and analysis of periodic planar liquid sheet assisted atomization

M. Averseng*, D. Zuzio*, A. Boutsikakis† and J.L. Estivalèzes*

*Multi-Physics Department for Energy - ONERA, 2 Avenue Edouard Belin, 31000 Toulouse, France

†Institut de Mécanique des Fluides de Toulouse (IMFT), Université de Toulouse, CNRS

2 Allée du Professeur Camille Soula, 31400 Toulouse, France

matthias.averseng@onera.fr - davide.zuzio@onera.fr - athanasios.boutsikakis@imft.fr - jean-luc.estivalezes@onera.fr*

Keywords: Air-blasted atomization, DNS simulations, liquid sheet, surface density

Abstract

Air-blasted atomization is the result of shearing instabilities triggered by the interactions between the liquid and gas flows. Many recent works have performed accurate Direct Numerical Simulation of liquid sheet disintegration. Indeed, high resolution DNSs are able to reproduce the smallest scales of atomization. Unfortunately this numerical accuracy is too expensive for industrial or parametric studies. LES is becoming on the other hand an efficient tool for simulating complex unsteady flows. However, in the case of assisted atomization no modelling is yet available for taking into account the sub-grid interfacial topological changes. A promising approach consists in building a transport equation for the sub-grid surface density, similar to the classical turbulence sub-grid quantities. In this approach, a source term takes in account the increase of the total liquid surface induced by the assisted atomization process. A definitive closure of this term is however not universally acknowledged. The objective of the present work is to contribute to the understanding and the modelling of the sub-grid surface source term. Several DNSs of a periodical planar liquid sheet atomization are presented, in which the total liquid surface evolution is measured in time. The influence of several inflow parameters, as density and velocity ratio, as well as initial boundary layer thickness, is evaluated on this quantity. Results show how surface growth rates as well as caracteristic times can be effectively measured in this kind of simulation.

Introduction

Atomization, or the process by which a coherent liquid disintegrates into droplets, is a fundamental topic of fluid mechanics. It is a highly complex process and substantial experimental and computational researchs have been carried out to understand the different stages of the atomisation process. Nowadays models for the so-called secondary atomization (the breakup of small liquid drops or structures into smaller droplets) are available and well-known but the description of primary atomization (the disintegration of a coherent liquid core into drops) is not enough mature. Indeed numerical modelling of primary break-up of a liquid structure (jet, sheet etc) is very challenging, especially for the conditions relevant to air/blast atomisation, highly turbulent flows, strongs aerodynamics forces and high liquid/gas density ratio.

Numerical methods that accurately describe the interface in two phase flows have become available in the last decade. Nowadays it is possible to carry out direct numerical simulations of the flow involving both phases and the interface. This permits the collection of very detailed information. Recent DNS studies have successfully described the primary atomization of liquid jets and cross-flows (Menard et al. (2007), Herrmann (2009), Shinjo & Umemura (2010), Desjardins & Pitsch (2010), Desjardins et al. (2013), O. McCaslin & Desjardins (2014), Ham et al. (2014), Sauer et al. (2014), Yue Ling et al. (2017), Odier et al. (2015), Zandian et al. (2016)). Some DNS studies have used an adaptative mesh refinement to optimize the computational costs (Agbaglah et al. (2011), Fuster et al. (2009), Zuzio (2010)) but in any case the numerical cutoff scale remains. Indeed the finest scale in multiphase flows remains unknown, contrary to the Kolmogorov and the Bachelor scale in single-phase flows. DNS of liquid jet atomization for industrial applications will remain out of scope in the near future due to excessive computational cost stemming from a large range of length and times scales.

For industrial application, computational cost as well as calculation time must be lower than DNS, that is why Large Eddy Simulation (LES) simulations are preferred. The numerical cutoff scale issue in the finest DNS proves the necessity of subgrid models. Indeed it is essential to modelize the physics under this particular scale and this logic is particularly true for LES simulations which use coarsed meshes than DNS. Recently LES of two phase flows have been investigated in few studies. The first approach used interface track-

ing methods to solve the interface without solving the finest scales of wrinkling (Labourasse et al. (2007)). Another more phenomenological approach, is to describe continuously the transition between a well resolved interface and structures smaller than the cell size. This approach introduces the interface density, which indicate the quantity of interfacial area in a given volume of control, but without indications on the shape of the structures. In the aforementioned study, Chesnel et al. (2011), adapted the ELSA model (initially proposed by Vallet & Borghi (1999)) to LES modeling, producing interesting statistical results independent of mesh size and in accordance with a reference two-phase flow.
The aim of this paper is to identify the most influencing parameters on primary atomization. Knowing them, it will be easier to target the atomization regime desired, such as ligament stretching, and to study it with the direct numerical simulation. Indeed the final objective is to implement a new subgrid model based on interfacial density concept in an LES solveur.

Numerical setup

Problem description

The "one-fluid" formulation of the incompressible Navier-Stokes equations is adopted here to describe the motion of two fluids in the domain. The mass and momentum equation are solved under the constant density hypothesis, leading to the system, Equations (1 & 2).

$$\nabla \cdot \mathbf{U} = 0 \tag{1}$$

$$\frac{\partial \rho \mathbf{U}}{\partial t} + \nabla \cdot (\rho \mathbf{U} \otimes \mathbf{U}) = \nabla \cdot (-p\mathbf{I} + \mathbf{D}) + \mathbf{f} \tag{2}$$

where $\mathbf{U}$ is the velocity field, p is the pressure, $\mathbf{f}$ a volumetric force (such as gravity) and $\mathbf{D}$ the viscous stress tensor. As we consider two non miscible phases, the local fluid properties like density and viscosity are derived from the interface tracking method, which will be briefly summarized thereafter. While crossing the interface, viscous stress tensor and pressure follow the jump condition (Equation 3):

$$[(-p\mathbf{I} + \mathbf{D}) \cdot \mathbf{n}] = \sigma \kappa \mathbf{n} \tag{3}$$

where σ is the surface tension, κ is the local curvature, $\mathbf{n}$ the unit vector normal to the interface.

Numerical code DYJEAT

In this paper, the code DYJEAT is employed. This code, in development at ONERA-Toulouse since 2004, has been used on various configurations related to atomization, including challenging high-density ratio cases such as water/air liquid sheet or cross-flow jet atomization.
The interface is tracked by coupled Level-Set, Volume-of-Fluid method (Sussman et al. (1994)) to ensure accuracy and mass conservation. Coupling these two approachs allows us to benefits from the mass conservation of VOF method and good precision in geometrical properties calculation thanks to Level-Set used.
The Level Set function ϕ is defined as the signed distance between any points of the domain and the interface. The zero level curve of that function therefore provides the interface location. At the same time a color function χ from VOF method represents the volumetric percentage of one fluid given on each cell. These functions ($\epsilon = \phi/\chi$) are advected by a given velocity field $\mathbf{U}$

$$\frac{\partial \epsilon}{\partial t} + \mathbf{U} \cdot \nabla \epsilon = 0 \tag{4}$$

The Level Set method no longer remained a distance function when solving (Equation 4) because of the velocity gradients, $\|\nabla \phi\| \neq 1$. The redistance algorithm (Sussman et al. (1994)) has to modify the advected Level Set function, without altering the zero contour, to reimpose the $\|\nabla \phi\| = 1$. After each interface update the coupling between the Level-Set and VOF colour function is done. Indeed in each mixed cells, the interface is approximated by a plane (PLIC reconstruction by Youngs (1982)). The plane is oriented by the use of the surrounding Level-Set values, and shifted to ensure mass conservation using VOF variable. From the reconstructed plane, mass fluxes can be geometrically computed as described in Sussman & Puckett (2000). This treatment is applied in each direction using a splitting algorithm.

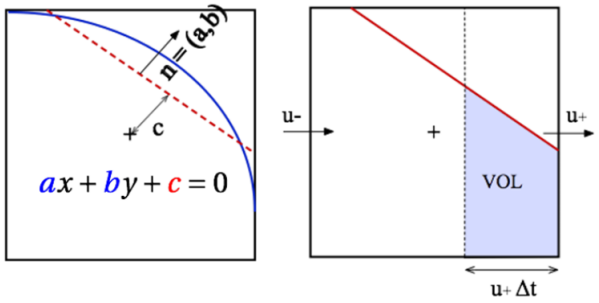

Figure 1: PLIC reconstruction and computation of mass flux through east face of a velocity cell.

Recently, a new method has been developed and implemented in DYJEAT by Orazzo et al. (2017), hereinafter referred as Conservative MOMentum (CMOM). The momentum equation is written in the conservative form (Equation 2) and treated with finite volume formulation. In the same way as for mass transport, momentum fluxes can be geometrically computed. The term $\rho\mathbf{U}$ is set equal to the mass fluxes calculated before since it appears in both advection terms: this treatment ensures consistency between mass and momentum conservation, and in that way provides the code with good robustness, even for high density ratio cases. This translates numerically to the resolution of conservative forms for both Equations (5 & 6):

$$\frac{\partial \rho}{\partial t} + \nabla \cdot (\rho \mathbf{U}) = 0 \tag{5}$$

$$\frac{\partial \rho \mathbf{U}}{\partial t} + \nabla \cdot (\rho \mathbf{U} \otimes \mathbf{U}) = \mathbf{RHS} \tag{6}$$

Pressure and stress tensor jumps, including surface tension, are taken into account by using a Ghost-Fluid method (Fedkiw et al. (1992)). In this method, the jumps are directly incorporated in the numerical discretization, by extending the

continuous solution behind the interface, and adding a source term to take in account the discontinuity: this ensures proper discretization on both sides of the interface and a sharp jump representation. In Figure 2, a simple 1D case is considered.

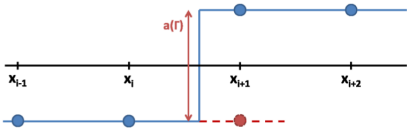

Figure 2: A jump across the interface taken into account with Ghost fluid formulation

In this example, the studied function is piecewise constant, with a jump at the interface between points x_i and x_{i+1} . The derivative is zero in each domain. To approximate the derivative at the right of point x_i , the monopasic version would simply be :

$$\left(\frac{dF}{dx}\right)_{i+\frac{1}{2}} = \frac{F_{i+1} - F_i}{x_{i+1} - x_i} \tag{7}$$

which is here obviously non zero. The idea of the ghost fluid method is to substitute value at the point F_{i+1} by its ghost value defined by

$$F_{ghost,i+1} = F_{i+1} - a_\Gamma \tag{8}$$

where a_Γ is the jump of F while crossing the interface. Calculating the jump a_Γ is made possible by explicitly locating the interface with the help of the surrounding Level-Set values. The discretization then results in the single-phase formulation corrected by a jump term. The Level-Set function is used to compute the interface normal vector and the courbure

VOFTOOLS library

The VOFTOOLS library was developed by López & Hernández (2008). It allows to perform a set of geometrical operations related to the VOF-PLIC interface reconstruction. Within this work, it is used to evaluate the liquid surface within each computational cell. Indeed, the interface in every cell is represented by a plane that can intersect with the cubic cell up to a maximum of six points, depending on how many faces of the cube it meets, as shown in Figure 3

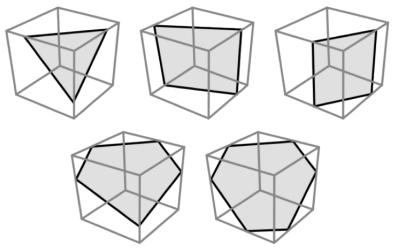

Figure 3: The five non-degenerate cases of a plane-cube intersection: triangle, parallelogram, pentagon, hexagon

Therefore, in order to calculate the surface of the resulting polygon, we simply apply the Stokes' theorem as shown in Schneider & Eberly (2003). Hence, we calculate the surface as the half dot product of the vector normal to the surface and the sum of the cross products of the (R^n) n-sided polygon's (Figure 4) vertices position vectors.

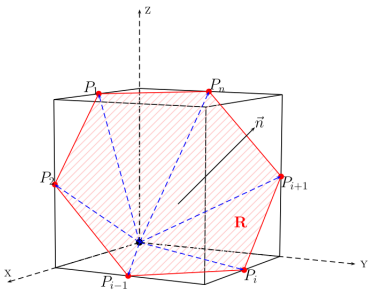

Figure 4: Interface polygon and intersection points in the context of VOFTOOLS.

$$A(R^n) = \frac{1}{2} \mid \hat{n} \cdot \sum_{i=0}^{n-1} (P_i \otimes P_{i+1} \mid, \quad 3 \leq n \leq 6 \tag{9}$$

Therefore, the liquid volume in a cell and the interface surface are calculated as

$$V_{li}^{VT} = \alpha_i \, V_i \tag{10}$$

$$S_{li}^{VT} = A(R_i^n) \tag{11}$$

Integral liquid volume and surface can be therefore computed by the sum of Equations (10 & 11) over the whole computational domain.

Geometrical configuration

The study of the air-blast atomization phenomenon was focused on a simplified but pertinent case, a periodical sheared planar liquid sheet. Although most realistic injection devices may rely on more complex configurations, the computational requirement of a planar liquid sheet simulation is typically lower because of the additional homogeneous periodic direction. Naturally, some features of round liquid jets such as Rayleigh instabilities, will be missing from the planar liquid simulations; however, it is expected that most aspects of the flow will be similar. In this study the liquid sheet is advected with a relatively small velocity and sheared by a fast parallel gas flow. The simulation was carried out in a three dimensional domain fully periodic, Figure 5.

Density and dynamic viscosity are respectively designated by ρ_l and μ_l for the liquid phase, and by ρ_g and μ_g for the gas. Surface tension is noted σ. The notation L_x, $L_y = L_x/2$ and $L_z = 2L_x$ represent repectively the lengh in streamwise (x), spanwise (y) and vertical (z) direction. The liquid sheet and boundary layer thickness are respectively noted α and δ.

A reference simulation set-up has been chosen between "stretched ligament" and "thorn-sheet" breakup regimes (Gutiérrez (2010)). The relative fluid characteristic are shown in Table 1 :

These fluids properties are imposed to simulate the behaviour

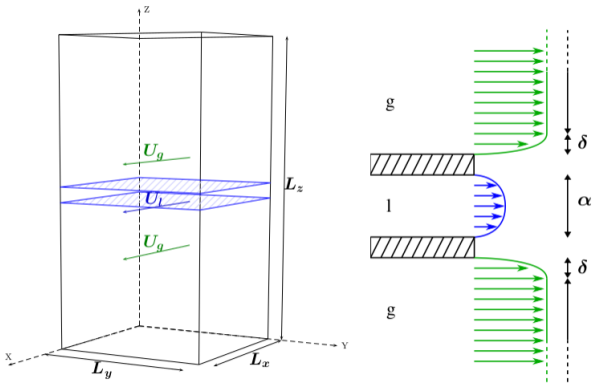

Figure 5: Computational domain & section (x, z) of the liquid sheet configuration

$U_l - U_g$	$\rho_l - \rho_g$	$\mu_l - \mu_g$	σ
$2 - 50$	$10^3 - 12$	$1.002\,10^{-3} - 1.8\,10^{-5}$	$7.2\,10^{-2}$
m/s	kg/m^3	$Pa.s$	$N.m$

Table 1: Fluids characteristics for the reference case

of water sheared by a faster and high-pressure surrounding air flow.
Several adimensional numbers can be used to characterize the atomization regime. However, as it is difficult to characterize sheet atomization behaviour by non-dimensional numbers alone, the parametric study will be performed by individually changing the dimensional parameters.

$$Re_l = \frac{\rho_l U_l \alpha}{\mu_l} \; Re_g = \frac{\rho_g U_g \delta}{\mu_g} \; We = \frac{\rho_g \left(U_g - U_l\right)^2 \alpha}{\sigma} \quad (12)$$

$$\hat{\mu} = \frac{\mu_g}{\mu_l} \qquad \hat{\rho} = \frac{\rho_g}{\rho_l} \qquad M = \frac{\rho_g U_g^2}{\rho_l U_l^2} \quad (13)$$

Re_l	Re_g	We	$\hat{\mu}$	$\hat{\rho}$	M
598.8	5000	115.2	$1.79\,10^{-2}$	$1.2\,10^{-2}$	7.5

Table 2: Adimensional numbers for the reference case

Validation of VOFTOOLS library

As explained before, the VOFTOOLS library allows an explicit estimation of the liquid interface by computing the surface of the polygon represented by the intersection of the PLIC interface and the cell boundaries. Two simple test cases are hereafter presented, in order to validate the time-dependent computation of the surface in a closed simulation domain. The first test case involves a static drop, of which the known surface value has to be retrieved numerically. The second test case involves a liquid cube evolving towards the stable spherical shape under the capillary forces. The physical parameters are arbitrarily set in order to rapidly converge to the equilibrium solution.

Static droplet
The first step in order to validate the VOFTOOLS library is to calculate the area of a spherical static droplet. The simulation domain is a cube having a side of length $L_{x,y,z} = 20\ mm$. The spherical droplet is placed at the cube center, with its diameter imposed, $d_p = 10\ mm$. The gas and liquid velocities are null so no deformation of the liquid gas interface occurs. The surface estimation (S), highly related to the mesh precision $\Delta x, y, z$, quickly converges to its theoric value (S_{theo}), Figure 6.

Cells nbrs	16^3	32^3	64^3	128^3	256^3	512^3
$\Delta x, y, z\ (mm)$	$\Delta = 1.25$	$\frac{\Delta}{2}$	$\frac{\Delta}{4}$	$\frac{\Delta}{8}$	$\frac{\Delta}{16}$	$\frac{\Delta}{32}$

Table 3: Cells numbers and grids sizes

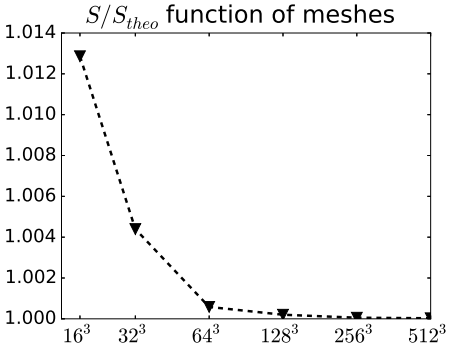

Figure 6: Adimensional droplet surface (triangle black dotted line) function of meshes

In order to retrieve the accuracy of the surface computation, the relative surface error $(er_{surface})$ is computed in function of the $d_p/\Delta x$ and the order p.

$$er_{surface} = a\,(d_p/\Delta x)^p \quad (14)$$

$$\log_{10}(er_{surface}) = c + p|\log_{10}(d_p/\Delta x)| \quad (15)$$

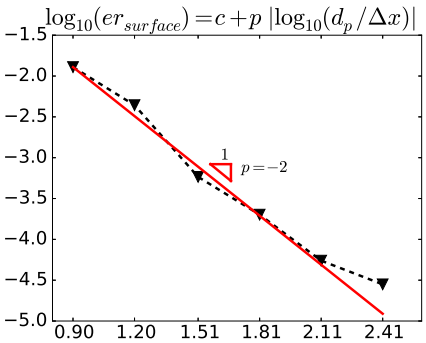

Figure 7: Convergence of the relative surface error with meshes

The higher relative surface error value is close to 10^{-2} (triangle black dotted line) and it is for the coarser mesh (16^3). The computed surface shows a second-order convergence towards the theoretical solution, Figure 7.

Static cube submit to surface tension

In this particular test case a static cube (of side length a) is initialized. The cube evolves under the surface tension and viscous forces towards the equilibrium spherical shape, Figure 8.

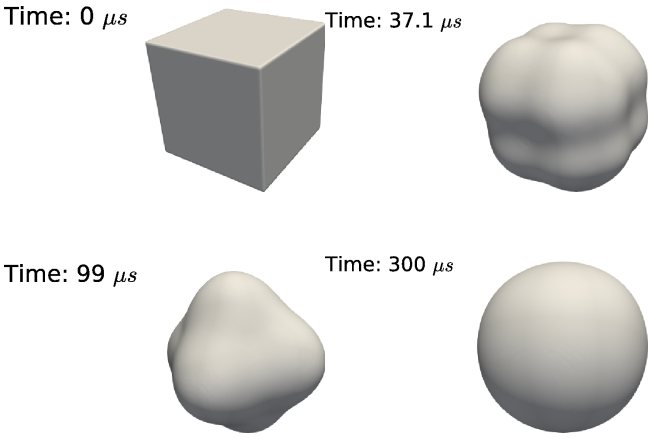

Figure 8: Surface changement caused by the surface tension

The initial surface is known and the final is easily predicted (spheric approximation) thanks to the volume conservation.

$$V_{cube} = a^3 \qquad S_{cube} = 6a^2 \tag{16}$$

$$V_{sphere} = V_{cube} \qquad S_{sphere} = 4\pi \left(\frac{3V_{sphere}}{4\pi} \right)^{2/3} \tag{17}$$

The geometrical and fluids characteristics are summed up in the following table, Table 4

$L_{x,y,z} - a$	N_{cells}	U_l	ρ_l	μ_l	σ
$4 - L_x/2$	128^3	0	1	$1.002.10^{-1}$	72
mm	$-$	m/s	kg/m^3	$Pa.s$	$N.m$

Table 4: Geometrical and liquid characteristics

The relative error in the surface computation is shown at the beginning (cube) and the end of the simulation in Table 5. The final error is less than one percent for the spherical shape. The greater error at the beginning is probably due to the sharp edges of the cube.

	$t_{initial}$	$t_{converge}$
$er_{surface}$ (%)	2.7	0.82

Table 5: Relative surface error

Two-Dimensional sheet behaviour

DNSs of assisted atomization are very expensive, mainly in reason of the scale gap between the initial liquid body and the smallest atomized droplets. For this reason, simplified two-dimensional simulations were carried out by neglecting the span-wise direction, thus focusing the simulations on the longitudinal flapping motion. Thus, it was possible to evaluate the effect of several parameters. Figure 9 shows the similarity of behaviour of a 2D and a 3D sheet destabilization. Relevant differences start to appear at the transverse instability onset. Therefore, the 2D simulation were carried out up to the first breakup of the two-dimensional ligaments.

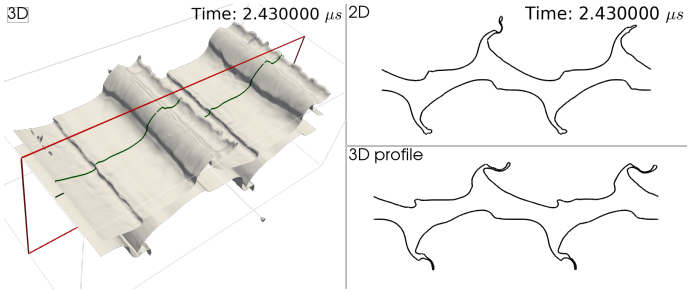

Figure 9: Comparisons between 3D/2D DNS

Mesh convergence

A convergence study was performed with the fluids characteristics established in Table 1. The computational domain size was set to $L_z = 2L_x$. A small velocity perturbation in the form of a sinusoidal function of wavelength $\lambda = L_x/2$ was added to accelerate the sheet destabilization. A non-dimensional number, related to the number of mesh points in the sheet thickness $\hat{\alpha} = \alpha/\Delta x$, was used and represents the mesh accuracy, Table 6.

$L_x - L_z - \lambda$	$\alpha - \delta - \hat{\alpha}$
$3 - 2L_x - L_x/2$	$300 - \alpha/2 - \alpha/\Delta x$
mm	μm

Table 6: Geometrical values

Different snapshots show the qualitative mesh influence in Figure 10. The coarser mesh ($\hat{\alpha} = 26$) acts as a low pass filter and smoothens much of the the smaller interfacial-instabilities compared to the finest grid ($\hat{\alpha} = 410$). The ejection of liquid structures is delayed.

This qualitative analysis is confirmed by the quantitative analysis of the surface production, showed in Figure 11 for

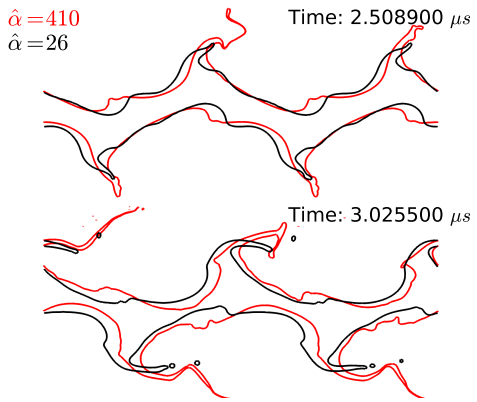

Figure 10: Snapshots of liquid sheet profiles for two meshes

different cells sizes. The curves show an increase in the detected surface growth as the mesh is refined. However, the results from the two finest meshes have converged. This results would indicate that the very small perturbations developing on the wave surface give the most contribution to the measured liquid surface.

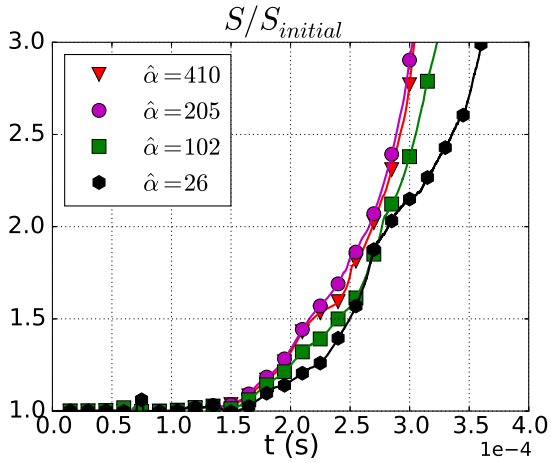

Figure 11: Surfaces measured function of meshes

The value $\hat{\alpha} = 205$ has therefore been chosen as the standard mesh for the subsequent parameter study.

Parametric study

As said previously, the computational domain is periodic. In consequence only few specific wavelengths linked to the domain size are take in account. As sheared liquid sheets destabilize under proper natural frequencies and wavelengths (Gutiérrez (2010), Couderc. (2006)), we want to avoid the imposition of arbitrary wavelengths which could in turn affect the instabilities growth. For this reason, the liquid sheet was initially perturbed with different wavelengths and the atomization process evolution (the surface production) was analysed. This perturbing velocity, function of the wavelengths, was formulated as follow :

$$v_{z_{pert}} = A\sin(2\pi x/\lambda) \quad A = U_l/20 \tag{18}$$

Figure 12 shows the influence of two different wavelengths on the interface production. The instability develops slower,

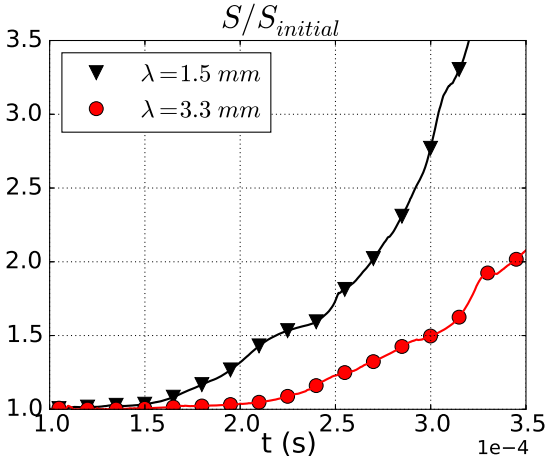

Figure 12: Wavelength effect on atomization process

with a much lower production rate.

In consequence, for each sheet configuration a variational study on the imposed wavelength has been performed by varying the computational domain size. Only the most unstable wavelength were retained for the rest of the study.

The sheet assisted atomization regimes (Stapper et al. (1990), Lozano et al. (2005)) mainly depend on the momentum flux ratio between air and liquid. The injector characteristics as well as the fluid properties, like viscosity and surface tension, also affect the outcome. In the proposed study, we investigated the parameters linked to the incoming air flow for two fixed fluids: the incoming air velocity, the gas density (linked to the pressure) and the boundary layer thickness. Purposefully, these parameters may represent a variation of throttle settings or altitude in the practical case of a combustion chamber. The variational study is resumed in Table 7

δ	ρ_g	U_g
$\{150, 250, 350\}$	$\{12, 24, 48\}$	$\{26, 34.2, 50\}$
μm	kg/m^3	m/s

Table 7: Parameters studied

The boundary layer effect was studied for each couple of parameters (U_g and ρ_g). Figure 13 shows an example of the effect of δ variation around the reference test case; the same effect was observed in the other operating points. An increment of the boundary layer thickness leads to a retarded atomization onset, but does not affect the surface growth rate.

Our proposed explanation is that the liquid body takes more time to reach the main air-stream, thus the delay. However, the atomization regime seems to remain the same in reason of the fixed momentum flux ratio M.

Subsequently, the gas density effect was studied. Indeed when the gas flow impacts and shears the liquid sheet with

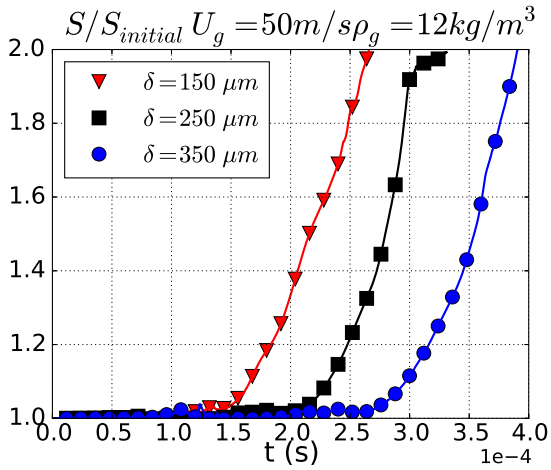

Figure 13: Boundary layer effect on atomization process

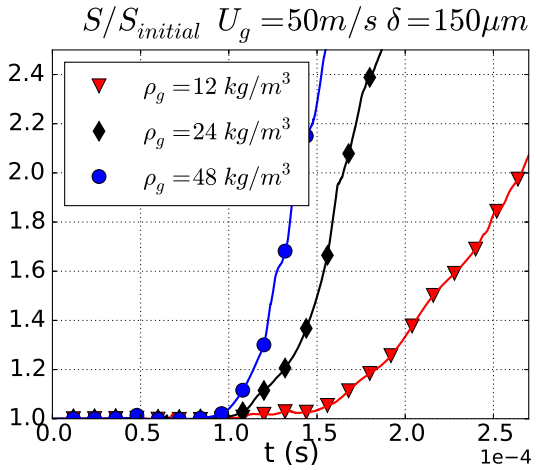

Figure 14: Density effect on atomization process

an a heavier weight, the kinetic energy transfer from the gas to the liquid increases. Figure 14 shows the effect on the surface growth rate: the higher pressure gas induces a stronger production rate, as more surface can be generated by the excess energy. The characteristic time of the sheet atomization is thus reduced.

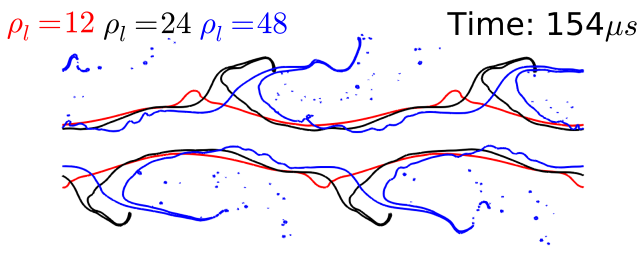

Figure 15: Liquid sheet profiles at $t = 154\ \mu s$

Figure 15 shows the different interface topologies at the same physical time. It is clear how with the higher gaz velocity the atomization process is well developed up to the formation of the droplet. The intermediate case show still forming ligaments, while in the lower density case the waves are still forming up. This explains the important differences in the surface curves of Figure 14: the most of the produces interface comes from the ligaments forming on the wave crests. Figure 16 shows the three simulations at the different physical times, but at the same quantity of produced interface. The same analysis was followed at iso $S = S_{init} = 1.6$ value. The same value of surface quantity is obtained with different mechanisms : smaller ligaments for the high density gas, and more pronounced main liquid body deformations for the low density case.

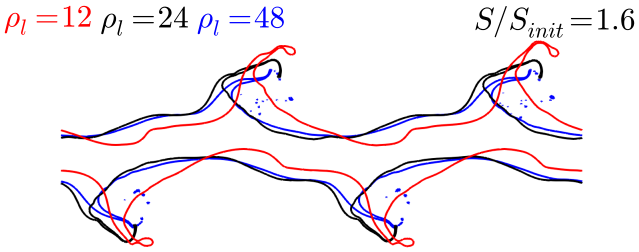

Figure 16: Liquid sheet profiles for $S/S_{init} = 1.6$

The last parameters analysed was the incoming gas velocity at iso δ and ρ_g values, the results shown in Figure 17. The general conclusion are the same than in the density study, an increase of the gas momentum flux by a greater velocity gives a better and earlier atomization, Figure 17.

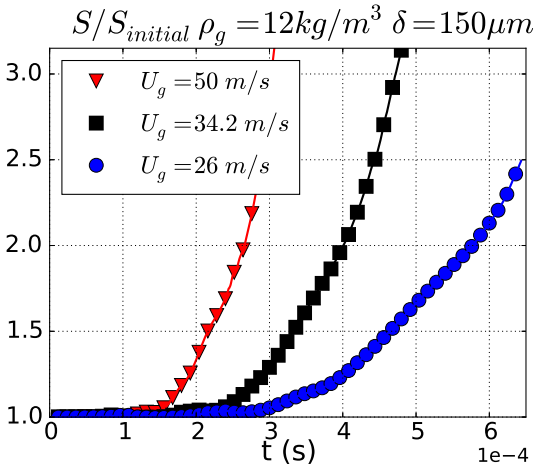

Figure 17: Velocity effect on atomization process

Figure 18 shows the three simulations at the different physical times, but at the same quantity of produced interface. The same analysis was followed at iso $S/S_{init} = 1.5$ value. The velocity influences and changes the process of atomization. In both cases ($U_g = \{34.2, 26\}$) the main liquid core is highly oscillating. On other hand the case ($U_g = \{50\}$) posses the same type of profile as said earlier, a main liquid core slightly oscillating while the waves quickly develop thin ligaments at their top, thus creating more surface than the other cases.

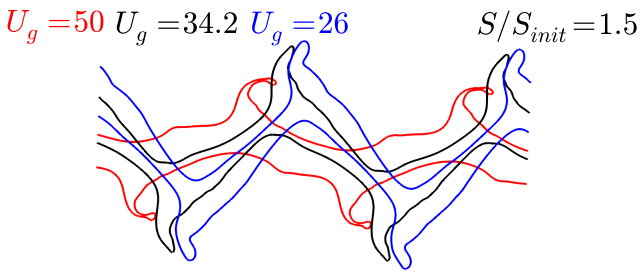

Figure 18: Liquid sheet profiles for $S/S_{init} = 1.5$

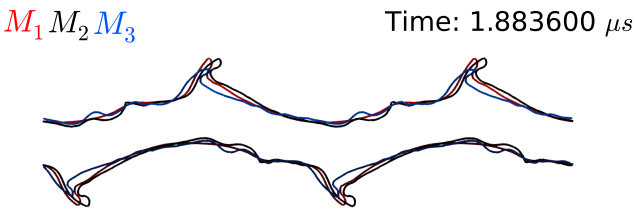

Figure 19: Liquid sheet profiles for meshes

Three-dimensional direct numerical simulation

A preliminary study was performed on three-dimensional simulations. Indeed, if the 2D simulations allowed for a detailed study of the longitudinal oscillation development, the mechanics leading to the final droplet formation consist mostly of three-dimensional phenomena. Indeed, the sheet develops transversal instabilities of smaller wavelength than the longitudinal one. These instabilities lead to the formation of the ligaments which in turn generate the droplets.

Mesh convergence

Simulations were carried out in the computational domain Table 8, with the fluids characteristics summed up in Table 1. A mesh convergence study was based on Table 9. A small velocity perturbation in the form of a sinusoidal function of wavelength $\lambda = L_x/2$ was added to accelerate the sheet destabilization.

$L_x - L_y - L_z$	$\alpha - \delta$
$3 - L_x/2 - 2L_x$	$300 - \alpha/2$
mm	μm

Table 8: Geometrical parameters

Meshes	M_1	M_2	M_3
$\Delta_{x,y,z}$	$L_x/1024$	$L_x/512$	$L_x/256$
N_{cells}	$1.07\ 10^9$	$134\ 10^6$	$16.7\ 10^6$
$\hat{\alpha}$	102	51	25

Table 9: Meshes parameters

Liquid core is well resolved by all the meshes as it can be seen Figure 19. Even in the coarser cases the spatial accuracy is high enough to catch all the large scales informations. Indeed, the surface production rate as well as the liquid sheet profile are similar, Figure 19, 20.

Conversely, the comparison of the meshes shows in Figure 21 how the transversal breakup is quite affected by the cell size. The finer mesh allows the formation of a continuous bulge at the crest of the wave, while in the coarsest mesh simulation breakup has already been triggered by the formation of holes. Therefore, In the next part only data extracted from the finest simulation were used.

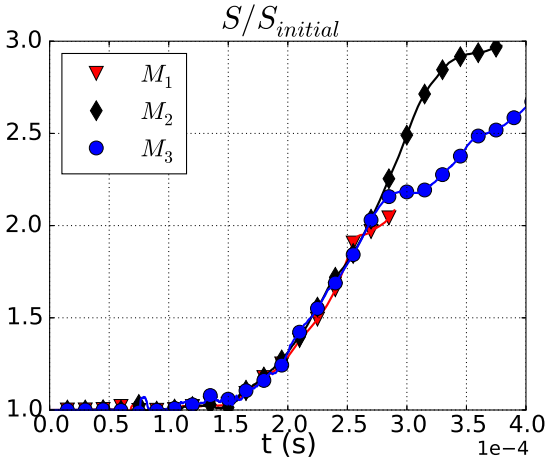

Figure 20: Liquid sheet profiles for velocities

Transversal instability

A formulation was proposed by Ben Rayana. (2007) to calculate this transversal instability on a planar installation:

$$\lambda_t = 2\pi\sqrt{\frac{6\alpha C}{C_d}}\delta_G \left(\frac{\rho_l}{\rho_g}\right)^{1/4} We_\delta^{-1/2} \tag{19}$$

Where α, C, C_d are coefficients, δ_G the boundary layer and We_δ the Weber number calculated from the boundary layer. The ligament number thus the computational size give the wavelength estimated in the simulation, Figure 22.

$$\lambda_{t_{BR}} = 120\ \mu m \tag{20}$$

$$\lambda_{t_{Simulation}} = \frac{L_y}{N_{ligament}} \simeq 150 \mu m \tag{21}$$

The estimated value is in good agreement with the Ben Rayana formulation. Further three dimensional simulations and relative analysis are planned, in order to characterize the transversal instabilities as well as the droplet formation. The first droplets are already visible in Figure 22. Dedicated algorithms will allow for a detailed analysis of the dispersed phase.

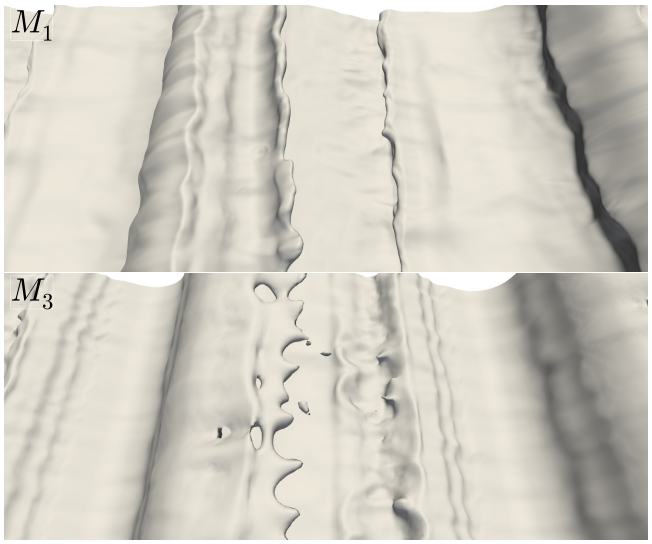

Figure 21: Wave crest development function of meshes

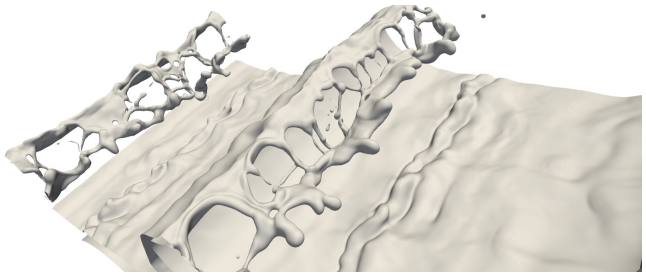

Figure 22: Transversal instability and ligament formation

Futur work & Conclusion

A preliminary numerical study was performed on the behaviour of a planar liquid sheet under assisted atomization. This works shows as the time-dependent total liquid surface can be computed and used to better understand the mechanisms underlying atomization. Many recent works propose RANS and LES modelling of atomization, often relying on dedicated transport equation for the subgrid interface density. The proposed DNS surface measurements may contribute to quantitatively evaluate the characteristic atomization times, the surface growth rate as well as critical Weber numbers used in this kind of large-scale modelling. Indeed, preliminary 2D study highlighted some different atomization process linked to some relevant parameters, as gas momentum and boundary layer thickness. That dependence and influence should be further investigated. Other quantites may also be investigated, such as the time-dependent integral liquid-gaz shearing velocity. This value could help linking the subgrid quantities to the local resolved velocity field.
Moreover, full spatial DNS of sheet atomization will be performed in order to fully develop the cloud of droplets. this kind of computation will allow a validation framework for the dedicated large-scale approaches.

Acknowledgments

Computer resources for this simulations have been provided by the CALMIP center (CALcul en MIdi Pyrénées).

References

Menard, T., Tanguy S., Berlemont, A., 2007 Coupling level set/vof/ghost fluid methods: validation and application to 3D simulation of the primary break-up of a liquid-jet. International Journal of Multiphase Flow 33(5), 510-524.

Shinjo, J., Umemura, A., 2010 Umemura Simulation of liquid jet primary breakup: dynamics of ligament and droplet formation. International Journal of Multiphase Flow 36(7), 513-532.

Desjardins, O., Pitsch, H., 2010 Detailed numerical investigation of turbulent atomization of liquid jets. Atomisation and Sprays 20(4), 311-336.

Herrmann, M., 2009 Detailed Simulations of the Breakup Processes of Turbulent Liquid Jets in Subsonic Crossflows. ICLASS.

Agbaglah, G., Delaux, S., Fuster, D., Hoepffner, J., Josserand, C., Popinet, S., Ray, P., Scardovelli, R., Zaleski, S., 2011. Parallel simulation of multiphase flow using octree adapivity and the volume-of-fluid method. Comptes Rendus Mécanique 339 (2-3), 194-207, High Performance Computing.

Fuster, D., Bagué, A., Boeck, T., Moyne, L.L., Leboissetier, A., Popinet, S., Ray, P., Scardovelli, R., Zaleski, S., 2009 Simulation of primary atomization with an octree adaptative mesh refinement and vof method. Internation Journal of Multiphase Flow 35 (6), 550-565.

Chesnel, J., Reveillon, J., Menard, T., Demoulin, F-X., 2011 Large eddy simulation of liquid jet atomization. Atomization and Sprays 21 (9), 711-736.

Vallet, A., Borghi, R., 1999 Modélisation eulerienne de l'atomisation d'un jet liquide. Compte Rendus de l'Académie des Sciences - Series IIB - Mechanics-Physics-Astronomy 327 (10),1015-1020.

Hirt, C.W., Nichols, B.D., 1981 Volume of fluid (Vof) method for the dynamics of free boundaries. Journal of Computatioal Physics 39 (1), 201-225.

Sussman, M., Smereka, P., Osher, S., 1994 A level set approach for computing solutions to incompressible two-phase flow. Journal Of Computational Physics 114 (1), 146-159.

Orazzo, A., Lagrange, I., Estivalèzes, J.-L., Zuzio, D., 2017 A VoF-Based Consistent Mass-Momentum Transport for Two-Phase Flow Simulations. ASME

Fedkiw, R.P., Aslam,T., Merriman, B., Osher, S., 1999 A non-oscillatory eulerian approach to interfaces in multimaterial flows (the ghost fluid method). Journal of Computational Physics 152 (2), 457-492.

López, J., Hernández, J., 2008 Analytical and geometrical tools for 3d volume of fluid methods in general grids. Journal of Computational Physics 227(12), 5939-5948

Schneider, P.J., Eberly, D.H., 2003 Geometric Tools for Computer Graphics. A volume in The Morgan Kaufmann Series in Computer Graphics. Elsevier Inc.

Zuzio, D., 2010 Direct numerical simulation of two phase flows with adaptive mesh refinement. PhD thesis, Institut Supérieur de l'Aéronautique et de l'Espace

Youngs, DL., 1982 Time dependent multi-material flow with large fluid distortion, Numerical Methods for Fluid Dynamics, KM Morton and MJ Braines, Academic Press, 273-285

Sussman, M., Puckett, E.G., 2000 A coupled Level Set and Volume-of-Fluid method for computing 3D and axisymmetric incompressible two-phase flows. Journal of Computational Physics, vol.162

Guttiérrez Fernández, V., 2010 Étude de l'atomisation primaire en haute pression. PhD thesis, Institut Supérieur de l'Aéronautique et de l'Espace

Desjardins, O., O. McCaslin, J., Owkes, M., Brady, P., 2013 Direct numrical and large eddy simulation of primary atomization in complex geometries. Atomization and Sprays, 23 (11): 1001-1048

O. McCaslin, J., Desjardins, O., 2014 Numerical investigation of primary air-blast atomization and modal analysis of flow instabilities. AIAA SciTech, National Harbor, Maryland 52nd Aerospace Sciences Meeting.

Ham, F., Kim, D., Bose, S., Le, H., Herrmann, M., 2014 Simulation of liquid fuel atomization by a complex high-shear swirling injector. Proceedings of ASME Turbo Expo 2014: Turbine Technical Conference and Exposition GT2014 June 16-20, 2014, DÃ$\frac{1}{4}$sseldorf, Germany

Ling, Y., Fuster, D., Zaleski, Z., Tryggvason, G., 2017 Spray formation in a quasiplanar gas-liquid mixing layer at moderate density ratios: A numerical closeup. Physical Review Fluids 2(1), 014005

Odier, N., Balarac, G., Corre, C., Moureau, V., 2015 Numerical study of a flapping liquid sheet sheared by a high-speed stream, International Journal of Multiphase Flow 77, 196-208

Zandian, A., Sirignano, W., Hussain, F., 2016 Three-dimensional liquid sheet breakup: vorticity dynamics, AIAA SciTech 4-8 January 2016, San Diego, California, USA 54th AIAA Aerospace Sciences Meeting

Sauer, B., Sadiki, A., Janicka, J., 2014 Embedded DNS concept for simulating the primary breakup of an airblast atomizer. Atomization and Sprays 26(3)

Labourasse, E., Lacanette, D., Toutant, A., Lubin, P., Vincent, S., Lebaigue, O., Caltagirone, J.P., Sagaut, P., 2007 Towards large eddy simulation of isothermal two-phase flows: Governing equations and a priori tests. International Journal of Multiphases Flow 33 (1), 1-39

Ben Rayana, F., 2007 Contributionà l'étude des instabilités interfaciales liquide-gas en atomisation assistée et tailles de gouttes. PhD thesis, Institut Supérieur de l'Aéronautique et de l'Espace

Couderc, F., 2007 Développement d'un code de calcul pour la simulation d'écoulements de fluides non miscibles. Application à la désintégration assistée d'un jet liquide par un courant gazeux. PhD thesis, Institut Supérieur de l'Aéronautique et de l'Espace

Lozano, A., Barreras, F., Siegler, C., Low, D., 2005 The effects of sheet thickness on the oscillation of an air-blasted liquid sheet. Experiments in Fluids 39: 127-139

Stapper, B.E., Sowa, W.A., Samuelsen, G.S., 1990 An Experimental Study of the Effects of Liquid Properties on the Breakup of a Two-Dimensional Liquid Sheet. Journal of Engineering for Gas Turbines and Power 114 (1)